Proceedings of the 1st SPAICE Conference on AI in and for Space | Pages 406 - 411 DOI: 10.5281/zenodo.13885637

Maximizing Celestial Awareness: 6-Synchronized-Star-Trackers for Attitude Determination

Aziz Amari*[1], Besma Guesmi[1], David Moloney[1]

[1] *Ubotica Technologies, Dublin, Ireland*

Attitude determination is a crucial task for space missions and relies on multiple onboard sensors such as sun sensors, magnetometers, and Earth horizon sensors. Moreover, star trackers, which identify stars in a scene and match them against an existing star catalog to determine the attitude, provide superior performance compared to traditional sensors and they were previously reserved for high-end missions. With the increasing popularity of small satellites, a trade-off between cost, efficiency, and precision is often encountered. Nowadays, star sensors have undergone significant advancements, becoming more efficient and accessible due to notable enhancements in hardware and software, particularly through the integration of neural networks. This leveraging of artificial intelligence (AI) has enabled the development of a compact and reliable star sensor, potentially eliminating the need for other sensor types. In this work, 6-synchronized star-trackers (6SST), a sensor with multiple imaging channels, is proposed to get wider celestial coverage and hence reliability. To justify this configuration, a more efficient and optimised software pipeline, along with an enhanced hardware implementation, is required.

1 Introduction

Reliability in space missions depends significantly on the On-board Attitude Determination System (OADS). As a fundamental component, the OADS plays an important role in ensuring the proper orientation and navigation of spacecraft. Thereby ensuring the success of missions and avoiding lost-in-space scenarios [1]. Attitude, defined as the three-dimensional orientation of a vehicle relative to a specific reference frame, is governed by the fundamental equations of motion for rotational dynamics. Consequently, the design of an OADS requires meticulous consideration of spacecraft geometry, mass properties, required accuracy, mission duration, hardware capabilities, and performance.

To estimate attitude, we use sensors that relate external references, such as the stars, the sun, the earth, or other celestial bodies, with the spacecraft's orientation. In most cases, we require the installation of various types of sensors, such as sun sensors, magnetometers, and earth horizon sensors, to ensure the reliability of the system, particularly considering that some sensors provide only two angles of attitude data [2]. The calculation of the third angle can be achieved by leveraging Kalman filtering [3], employing data from two different types of sensors.

In this work, we focus on Star-Trackers [4], optical sensors used in spacecraft and satellites to precisely determine the attitude relative to the stars. They ensure high accuracy and precision while providing the full three-dimensional attitude without requiring additional sensors. The typical workflow for Star-Trackers consists of capturing an image, extracting a series of centroids that represent stars that are then matched against a catalog of known stars in order to determine orientation.

Recently, small satellites and CubeSats have surged in popularity, driven by their affordability and simplified design [5] [6]. However, this trend brings about resource scarcity and performance constraints, especially considering that the traditional star sensor is a relatively complex system that was previously reserved for high-end missions. Thus, to attain the required attitude estimation precision in space missions low-cost and efficient star-trackers have emerged [7] [8].

We can also reduce complexity by removing other types of sensors and adopting a star-tracker-only approach [2] [9]. This is intuitive because having multiple sensors introduces mass and consumes scarce internal volume in the satellite that could be utilized for other purposes.

The demand for compact Star-Trackers has prompted the adoption of AI-based approaches [10]. Many studies have embraced the use of neural networks for tasks such as star identification [1] [11] and in centroid estimation [12], demonstrating the integration of AI into Star-Tracker development.

In this context, we propose the implementation of

*Corresponding author. E-Mail: aziz.amari@ubotica.com

6-synchronised-star-trackers (6SST), a sensor with six imaging channels, one for each face of a typical cubesat, operating in parallel, each providing a unique perspective. This setup enhances attitude determination reliability by providing tracking of the entire celestial sphere. Having wide celestial coverage opens up new possibilities [13], including but not limited to space debris cataloguing [14] [15], Space Situational Awareness (SSA) [16], and improved relative positioning for complex satellite formation flying maneuvers. However, this architecture requires highly efficient software and hardware implementation to justify the operation of a multifaceted sensor [17]. Our contribution consists of justifying this proposal by developing a more efficient light-performance pipeline, considering the management of onboard resources such as power and memory.

The remainder of this paper is structured as follows. In Section 2, we introduce the considered material and adopted methods. Section 3 discusses the results obtained. Finally, Section 4 concludes the paper and suggests ideas for future work.

2 Materials and Methods

In this section, we outline the materials and methods employed in our experimentation. We begin by detailing the data generation process, followed by an overview of the proposed approaches.

2.1 Materials

2.1.1 Data Generation

In our study, we utilised ESA's simulator provided in the Kelvins competition "Star Trackers: First contact". This simulator serves as a platform for generating synthetics star data by effectively filtering the Hipparcos [18] catalogue based on a predetermined magnitude threshold and generating relevant data tailored to the chosen simulation settings. Our generated dataset consists of 2300 images where each image is accompanied by a corresponding file containing (x,y) coordinates relative to the image for every star within the frame, as well as the scene's exact attitude in space. In our context, attitude is represented by a 3-tuple (Right Ascension ω, Declination ψ, Roll). The Hipparcos catalogue uses celestial coordinates (ω, ψ) for the epoch J1991.25 [19] [20], while roll refers to the rotation around the line of sight of the observing spacecraft. When determining the simulation parameters, we drew upon insights from the research conducted by Rijllarsdam et al. [21] as can be seen in Table 1.

Parameter	Value
Field of view (FOV) of camera	20x20 degrees
Normalized Focal Length (f)	2.836
Normalized Principal Point p_x, p_y	0.5
Sigma PSF	0.5 pixel
Exposure Time	0.2 s
Cut-off magnitude Threshold	$5.3\,M_v$
Magnitude Gaussian	$0.01\,M_v$

Table 1: Simulation parameters.

2.1.2 Noise Addition

On-board imaging systems produce images with a low signal-to-noise ratio [22]. This is caused by various physical constraints, such as faint incoming light and analog-to-digital data conversion. Multiple noise models [23] can be present. Following Guesmi et Moloney's work [24], different noise models are generated such as salt and pepper, Read, Shot, and Gaussian noise to handle real conditions. Table 2 presents the parameters we adopted.

Parameter	Value
Salt Probability	0.003
Pepper Probability	0.007
Read Mean	0
Read Standard Deviation	4
Gaussian Mean	3
Gaussian Sigma	1.3

Table 2: Added Noise Parameters

2.1.3 Multi-Faced Images

Considering the availability of multiple data sources, image stitching becomes a viable choice for improving performance. This allows us to construct a wide field-of-view (FOV) scene by stitching together multiple images with limited FOV, effectively eliminating redundant information. Thus, this process is simulated by utilizing a Python script to generate six translated and rotated point-of-views from a given image to generate overlapped data from different angles.

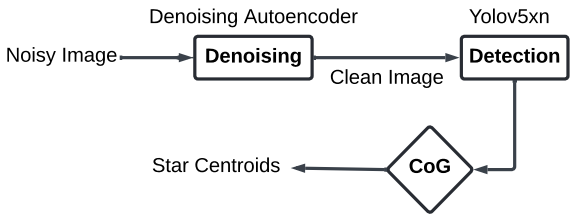

Figure 1: Star denoising and detection pipeline proposed in [24].

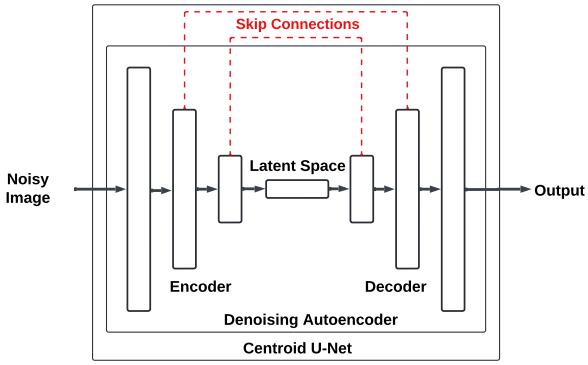

Figure 2: Proposed star detection U-Net-based Denoising Autoencoder architecture.

2.2 Methods

2.2.1 End-to-End Detection

Previously, a denoising autoencoder has been proposed to reconstruct clean star images, a lightweight modified yolov5x to estimate the bounding boxes of small objects (stars) [24] and then compute the Center of Gravity (CoG) of every bounding box to get the star centroid as illustrated in Figure 1. The aim of our work is to propose a lightweight but efficient star detection pipeline for accurate centroiding and attitude determination. Firstly, the denoising autoencoder proposed in [24] is trained for image denoising, and then the decoder layers are removed because reconstructing the image is not necessary as the latent space contains all the information we need. Basically, we can use the encoder's output as input for training the star detection model. Instead of estimating bounding boxes [24], it makes sense to directly output the (x, y) coordinates and remove the CoG calculation step. Thus, we propose an end-to-end star model that accomplishes both tasks in a one-shot manner [25], image denoising and outputs a segmentation map estimation [26] for localizing stars. To achieve this we can adopt an Autoencoder-based U-Net architecture [27] with shared layers as you can see in Figure 2. A lightweight deep learning approach is justified over traditional image processing methods due to it addressing resource constraints while maintaining high performance. For instance, Dave et al. [15] introduced RSOnet, a CNN-based system that enables wide-FOV camera sensors for Resident Space Object (RSO) detection and tracking. This justifies the use of machine learning in our proposed framework, ensuring that we leverage these benefits for improved star detection.

2.2.2 Image Stitching

Fortunately, a lot of prior work [28] [29] has been done on image stitching due to its importance in domains such as medical imaging and remote sensing. The typical approach consists of matching the features extracted by methods like SIFT [30]. Then, the geometric relationships between the images need to be determined. The homography [31] transformation that takes you from one image to another. However, if we plan to use a homography matrix-based approach we won't need to calculate it again every time because the positions of our installed sensors are fixed. Thanks to having a considerable amount of data we can try out efficient deep learning methods for feature extraction [32] instead of relying on SIFT. In this context, Nie et al. [33] have proposed an efficient image-stitching approach. One of their key insights is the proposal of a novel composition approach to generate seamless stitched images via unsupervised learning. This method effectively eliminates parallax artifacts and avoids undesirable blurring compared to previous techniques. For this work, the composition task is expended to support six warped inputs, enabling the creation of a large wide star image panorama. This panorama serves as input to the 6SST pipeline, reducing processing resources while ensuring greater accuracy compared to using a single limited FOV image.

2.2.3 Attitude Determination Pipeline

For the purposes of this paper, we use an existing attitude determination method as an evaluation tool to study the effect of pixel shifting caused by denoising and stitching models, as presented in Section III. While we have yet to develop our own approach, this will be addressed in future work. After estimating the centroids in the image, we adopt the attitude determination pipeline presented in [21]. This method accounts for the trade-off between accuracy and complexity, employing neural networks for star identification followed by a verification step using the star catalog to estimate attitude.

3 Results and Discussion

3.1 Star shifting due to reconstruction

The analysis aims to understand the impact of our models on centroid estimation accuracy and to make sure that the denoising and stitching steps did not shift the stars which can introduce errors in the attitude estimation process. Since the dataset was simulated, we have the precise centroid for every star. The evaluation consists of drawing a 20x20 pixel bounding box around every star, calculating the CoG, and determining the average Centroid Estimation Error (CEE) across different image types Equation (1) [34] on different image types.

$$CEE = \frac{\sqrt{(x_c - x_c^*)^2 + (y_c - y_c^*)^2}}{S} \quad (1)$$

where (x_c, y_c) represent the ground truth centroid and (x_c^*, y_c^*) are the CoG calcualted centroids. S is the number of stars in the image. Table 3 shows that the

Image Type	Average CEE (px)
Ground Truth	0
Clean Image	0.329
Noisy Image	0.546
Denoised Image	0.576
Stitched Image	0.964

Table 3: Average centroid shifting results in pixels

centroid estimation process effectively localised stars within the provided bounding boxes, demonstrating robust performance. Despite going through the denoising autoencoder, the reconstructed image maintained a relatively stable centroid estimation, before and after denoising. On average, shifted centroids are less than one pixel off from the actual star centroids. This leads us to another question, how much shifting and lack of centroid precision is tolerable and what is the effect on attitude determination?

3.2 Shifting effect on Attitude Determination

The process consists of gradually adding random shifting to the ground truth star centroids of our test images and then comparing the estimated attitude with the correct value. By doing this we can learn how much imprecision and shifting in the detection and stitching pipelines we can tolerate.

$$\text{Random Shifting } (x, y, r) = (x + r_1, y + r_2) \quad (2)$$

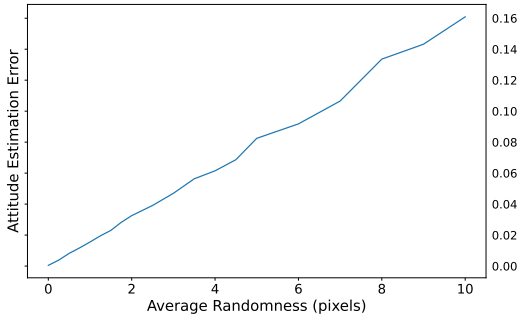

Figure 3: Correlation between the average randomness and the attitude estimation error.

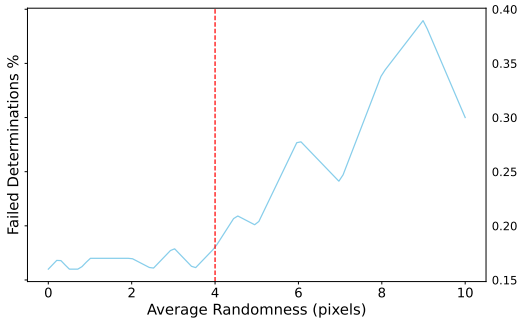

Figure 4: Relationship between the average randomness and the percentage of failed attitude estimations.

Random shifting is calculated according to Equation (2), where r_1 and r_2 are random variables representing the shift in the x and y directions, respectively. These random variables are drawn from a distribution with an average randomness r, where $0 \leq r \leq 10$ pixels. It is intuitive to expect a positive correlation between the average randomness and the average attitude determination error. Instead of making assumptions, we empirically verify this through Figure 3. To determine the tolerable degree of shifting, we compared the percentage of failed determinations to the degree of imprecision we added. As depicted in Figure 4, there is a significant increase in failure after 4 pixels of imprecision.

3.3 Six Views Stitching

The warped model achieved impressive stitching results, reaching a total loss of 0.0076 within only 5 epochs. Initially, the model was trained on a dataset consisting of 2 views, each containing 2603 samples. These results demonstrate the efficiency and accuracy of the model in producing seamless stitched images from multiple perspectives. Subsequently, the composition task was performed, producing stitched images

that represent the full panorama of six views.

4 Conclusion

The novelty of this study revolves around the notion that achieving complete celestial coverage enhances the reliability of star trackers for attitude estimation and unlocks possibilities for tasks such as space debris cataloguing, space situational awareness, and complex satellite formation flying maneuvers. Despite the inherent challenges in implementing a 6SST system, particularly concerning software and hardware efficiency, our study and preliminary findings underscore its potential call for further exploration. Looking ahead, our efforts will encompass exploring additional applications, refining software implementation, and conducting comprehensive benchmarking across various hardware systems to compare metrics like inference time, data rate, and power consumption, which will allow us to select a suitable System-on-Chip. Leveraging AI-optimized hardware, we can further emphasize the feasibility of the proposal. Additionally, future work will include providing detailed information on the optical system, such as the field of view (FOV) and the relative orientation of the six imaging channels. We will specify the choice of sensors and the onboard computer used, as well as include the overall physical dimensions resulting from implementing six imaging pipelines. We will also discuss any challenges these dimensions might pose for space utilization.

References

1. Rijlaarsdam, D. *et al.* A Survey of Lost-in-Space Star Identification Algorithms Since 2009. *Sensors* **20.** ISSN: 1424-8220. https://www.mdpi.com/1424-8220/20/9/2579 (2020).
2. Enright, J., Sinclair, D., Grant, C., McVittie, G. & Dzamba, T. Towards star tracker only attitude estimation (2010).
3. Sun, S.-l. Multi-sensor optimal information fusion Kalman filters with applications. *Aerospace Science and Technology* **8,** 57–62 (2004).
4. Liebe, C. C. Star trackers for attitude determination. *IEEE Aerospace and Electronic Systems Magazine* **10,** 10–16 (1995).
5. Ofodile, I. *et al. ESTCube-2 attitude determination and control: Step towards interplanetary CubeSats* in *2019 IEEE Aerospace Conference* (2019), 1–12.
6. Janson, S. & Welle, R. The NASA optical communication and sensor demonstration program (2013).
7. Samaan, M. & Theil, S. Development of a low cost star tracker for the SHEFEX mission. *Aerospace Science and Technology* **23,** 469–478. ISSN: 1270-9638. https://www.sciencedirect.com/science/article/pii/S1270963811001684 (2012).
8. Ho, K. A survey of algorithms for star identification with low-cost star trackers. *Acta Astronautica* **73,** 156–163. ISSN: 0094-5765. https://www.sciencedirect.com/science/article/pii/S0094576511003195 (2012).
9. Critchley-Marrows, J. J. R., Wu, X. & Cairns, I. H. Treatment of Extended Kalman Filter Implementations for the Gyroless Star Tracker. *Sensors* **22.** ISSN: 1424-8220. https://www.mdpi.com/1424-8220/22/22/9002 (2022).
10. Carmeli, G. & Ben-Moshe, B. AI-Based Real-Time Star Tracker. *Electronics* **12.** ISSN: 2079-9292. https://www.mdpi.com/2079-9292/12/9/2084 (2023).
11. Wang, B., Wang, H. & Jin, Z. An Efficient and Robust Star Identification Algorithm Based on Neural Networks. *Sensors* **21.** ISSN: 1424-8220. https://www.mdpi.com/1424-8220/21/22/7686 (2021).
12. Zapevalin, P., Novoselov, A. & Zharov, V. Artificial neural network for star tracker centroid computation. *Advances in Space Research* **71,** 3917–3925. ISSN: 0273-1177. https://www.sciencedirect.com/science/article/pii/S0273117722010456 (2023).
13. Dikmen, S. *Development of star tracker attitude and position determination system for spacecraft maneuvering and docking facility* 2016.
14. Liu, M. *et al.* Space Debris Detection and Positioning Technology Based on Multiple Star Trackers. *Applied Sciences* **12.** ISSN: 2076-3417. https://www.mdpi.com/2076-3417/12/7/3593 (2022).
15. Dave, S., Clark, R. & Lee, R. S. K. RSOnet: An Image-Processing Framework for a Dual-Purpose Star Tracker as an Opportunistic Space Surveillance Sensor. *Sensors* **22.** ISSN: 1424-8220. https://www.mdpi.com/1424-8220/22/15/5688 (2022).
16. Kennewell, J. A. & Vo, B.-N. *An overview of space situational awareness* in *Proceedings of the 16th International Conference on Information Fusion* (2013), 1029–1036.
17. Opromolla, R. *et al.* A new star tracker concept for satellite attitude determination based on a multi-purpose panoramic camera. *Acta Astronautica* **140,** 166–175 (Aug. 2017).
18. Perryman, M. Astronomical Applications of Astrometry: Ten Years of Exploitation of the Hipparcos Satellite Data. *Astronomical Applications of Astrometry: Ten Years of Exploitation of the Hipparcos Satellite Data* (Jan. 2008).
19. Perryman, M. A. *et al.* The HIPPARCOS catalogue. *Astronomy and Astrophysics, Vol. 323, p. L49-L52* **323,** L49–L52 (1997).
20. Xu, M. H., Wang, G. L. & Zhao, M. A new concept of the International Celestial Reference Frame: the epoch ICRF. *Monthly Notices of the Royal Astronomical Society* **430,** 2633–2637. ISSN: 0035-8711. eprint: https://academic.oup.com/mnras/article-pdf/430/4/2633/3823372/stt044.pdf. https://doi.org/10.1093/mnras/stt044 (Feb. 2013).
21. Rijlaarsdam, D. *et al.* Efficient Star Identification Using a Neural Network. *Sensors* **20,** 3684 (June 2020).
22. Wi, J., Baeck, K. & Yoon, H. Modeling and Filtering Colored Noise of a Star Tracker. *The Journal of the Astronautical Sciences* **70,** 8. ISSN: 2195-0571. https://doi.org/10.1007/s40295-023-00376-w (2023).
23. Boyat, A. K. & Joshi, B. K. A Review Paper: Noise Models in Digital Image Processing. eprint: arXiv:1505.03489 (2015).
24. Guesmi, B. & Moloney, D. *Hardware-aware, deep-learning approaches for image denoising and star detection for star tracker sensor* https://www.embedded-world.de/en/conferences-programme/talque-plugin?talque=speaker-list&speakerId=jdpFNN1O1pnuRNpIYyZ1. 2024.
25. Crawshaw, M. Multi-Task Learning with Deep Neural Networks: A Survey. *ArXiv* **abs/2009.09796.** https://api.semanticscholar.org/CorpusID:221819295 (2020).

26. Brempong, E. A. *et al. Denoising pretraining for semantic segmentation* in *Proceedings of the IEEE/CVF conference on computer vision and pattern recognition* (2022), 4175–4186.
27. Chuang, C.-H., Chang, K.-Y., Huang, C.-S. & Jung, T.-P. ICU-Net: A U-Net-based Denoising Autoencoder Using Mixtures of Independent Components for Automatic EEG Artifact Removal. *NeuroImage* **263,** 119586. ISSN: 1053-8119. https://www.sciencedirect.com/science/article/pii/S1053811922007017 (2022).
28. LYU, W., ZHOU, Z., CHEN, L. & ZHOU, Y. A survey on image and video stitching. *Virtual Reality and Intelligent Hardware* **1,** 55–83. ISSN: 2096-5796. https://www.sciencedirect.com/science/article/pii/S2096579619300063 (2019).
29. Brown, M. & Lowe, D. G. Automatic Panoramic Image Stitching using Invariant Features. *International Journal of Computer Vision* **74,** 59–73. ISSN: 1573-1405. https://doi.org/10.1007/s11263-006-0002-3 (2007).
30. Lindeberg, T. Scale invariant feature transform (2012).
31. Luo, Y. *et al.* A Review of Homography Estimation: Advances and Challenges. *Electronics* **12.** ISSN: 2079-9292. https://www.mdpi.com/2079-9292/12/24/4977 (2023).
32. Adel, E., Elmogy, M. & El-Bakry, H. Image Stitching based on Feature Extraction Techniques: A Survey. *International Journal of Computer Applications* **99,** 1–8 (Aug. 2014).
33. Nie, L., Lin, C., Liao, K., Liu, S. & Zhao, Y. *Parallax-Tolerant Unsupervised Deep Image Stitching* in *2023 IEEE/CVF International Conference on Computer Vision (ICCV)* (IEEE Computer Society, Los Alamitos, CA, USA, Oct. 2023), 7365–7374. https://doi.ieeecomputersociety.org/10.1109/ICCV51070.2023.00680.
34. Akondi, V., Roopashree, M. & Prasad, B. Denoising Shack Hartmann Sensor spot pattern using Zernike Reconstructor. *International Journal of Power Control Signal and Computation* **2,** 119–123 (Sept. 2009).